MODELLING WAVE-STRUCTURE INTERACTION WITH A NEW COMPRESSIBLE TWO-PHASE FLOW SOLVER

Sara Mizar Formentin [1], Juan Carlos Alcérreca Huerta [2] and Barbara Zanuttigh[3]

This contribution presents and investigates the effects of the air entrainment and air compressibility on the shape and magnitude of the wave impacts occurring at crown walls on top of sea defenses. To this purpose, a new solver, developed in the OpenFoam environment to represent the wave interactions with impermeable and porous coastal structures, accounting for the fluid compressibility, is checked against recent laboratory tests of wave overtopping and wave impacts. By comparing the first results of this new code to the ones obtained with the native solver dealing with incompressible fluids exclusively, significant advances in the representation of the pressure signals and peaks at the walls seem to be achieved.

Keywords: air entrainment; fluid compressibility; two-phase flow; wave overtopping; wave impacts

INTRODUCTION

The wave action and its interaction with coastal structures generates pressure, loads and forces, which are extremely important to assess the overall stability. Particular attention has to be paid to the case of waves directly breaking against the structures, producing violent impacts which can compromise the proper functioning of the system and produce structural damages. Typically, this happens in case of vertical walls or very steep slopes, where the waves reach the structure unbroken and where the violence of the impact is enhanced by the formation of air bubbles entrapped in the water phase beneath the impinging wave. The trapped air interacts with the surrounding fluid in a pulsating motion wherein the fluid energy is alternatively stocked and released, generating subsequent phases of compression and expansion of the aerated water (Bullock et al., 2007). This causes oscillations in the load-pressure signals, which are damped afterwards due to the leakage of the trapped air and the disintegration of the air pocket into a bubbly flow. The relevance of the air pockets on the distribution and on the intensity of the wave pressures at seawalls is demonstrated in several studies (Peregrine et al., 2005). The experimental investigation of the air entrainment is however quite expensive and affected by scale effects (a.o.: Cuomo et al., 2010; Bredmose et al., 2015). Previous numerical studies on the effects of flow compressibility focused on short wave-trains or on regular waves (Plumerault et al., 2012; Ma et al., 2014; Liu et al., 2019), while the representation of long time series of irregular waves is needed for design purposes (McKenna and Allsop, 1999).

Strong effects of the air compressibility are also evident in the dynamics of two-phase flows in porous media, as for example in the case of permeable breakwaters subjected to run-up and overtopping. In such conditions, the flow across the pores of the structure is governed by the classical Navier-Stokes equations and the Darcy-Forchheimer's equation, but it cannot disregard, realistically, the effects induced on the flow by the compression/expansion of the air cushions entrapped in the pores subsequent to the up-rush and up-down of the waves. Up to the authors' best knowledge, no numerical model is today available accounting for, contemporarily, the wave generation/absorption, the fluid compressibility and the flow across porous/impervious structures or layers. Such a tool would be fundamental for the improvement of the knowledge regarding wave–structure interactions towards the development and the optimal design of innovative marine structures for harbour protection and energy production.

Starting from this observation, this paper presents the earlies results of a new compressible solver recently developed in the OpenFoam environment that is going to be released to scientific community. After briefly describing its governing equations and main features, such solver is applied here to simulate nearly 500 s of irregular waves overtopping an impermeable dike and impacting against a crown wall situated on top of the dike. The results of the code are investigated in terms of hydraulic parameters, wave overtopping discharge and wave pressures and compared with the corresponding results of the laboratory test and the original incompressible OpenFoam solver is carried out. A detailed analysis of

[1] DICAM – Università di Bologna, Viale del Risorgimento 2, Bologna, 40123, Italy
[2] Consejo Nacional de Ciencia y Tecnología-El Colegio de la Frontera Sur (CONACYT-ECOSUR), Department of Observation and Study of the Land, the Atmosphere and the Ocean, Av. Del Centenario km 5.5, Chetumal, Quintana Roo, 77014, Mexico.

the wave loads occurring at the walls under low- and high-aerated conditions is proposed, to show the effects of the aeration on the pressure trace and magnitudes. Finally, the evolution of the air entrainment from the wave breaking over the dike berm to the wave impact against the wall is shown with the support of image analysis.

NUMERICAL MODEL

The present section aims to describe the different steps for the development of CFD solvers capable to simulate generate/absorb surface water waves by considering the compressibility of the fluids, which could be relevant in the wave – porous/impermeable structure interactions.

Model description

The numerical model developed is based on the CFD toolbox OpenFoam® and existing libraries coupled with native solvers for the implementation of wave generation/absorption. The basis of the numerical model is stablished upon the time – averaged equations of fluid motion given by the Reynolds – Averaged Navier Stokes (RANS) equations, where the instantaneous velocities are decomposed into a mean (time – averaged) and a fluctuating term following the Reynolds decomposition. To describe surface wave motions near structure, which could be either impervious or a permeable or a combination of both, the Volume – Averaged Reynolds Averaged Navier Stokes (VARANS) should be implemented. Therefore, by considering porosity effects and fluid compressibility, the VARANS equations are described as in Eq. 1 and Eq. 2 for the continuity and momentum equations, respectively:

$$\frac{\partial \rho}{\partial t} + \frac{1}{n} \nabla \rho U = 0 \tag{1}$$

$$\frac{1}{n}\frac{\partial \rho U}{\partial t} + \frac{1}{n^2} \nabla (\rho U U) = -\nabla p + \frac{1}{n} \nabla \mu_{eff} \nabla U + F_s - F_p \tag{2}$$

where U is the velocity, p the total pressure, n the porosity, and μ_{eff} is the viscous term that, according to the Reynolds decomposition, results from the contribution of the dynamic and turbulent viscosity ($\mu_{eff} = \mu + \mu_t$).

The term F_s stands for the effects of surface tension between fluids, described as $Fs = \sigma \kappa \alpha$, with σ the surface tension coefficient between fluids, κ the curvature of the interface, and α the vector normal to the fluid-fluid interface. Also, the term Fs represents the porous media effects over the fluid motion. It could be described as in Eq. 3, following the Darcy-Forchheimer equation and the Polubarinova – Kochina term (PK – term), that include the time derivative to account for the added mass effect:

$$F_p = aU + b|U|U + c_A \frac{\partial \rho U}{\partial t} \tag{3}$$

In Eq. 3, the coefficients a, b, and c_A are defined based on existing empirical approximations to model the porous media (e.g. Ergun, 1952; Engelund, 1953; van Gent, 1995).

The VOF method is used in the numerical model to track the fluids interface, for which the fluid fraction (α) in a computational cell is α=1 for one of the fluids (fluid phase 1) and α=0 for the other (fluid phase 2), so that the interface is located at α=0.5.

A diagram of the existing solvers developed within the OpenFOAM framework is shown in Figure 1, where the implementation of the wave generation/absorption of regular and irregular wave trains as a boundary condition (Jacobsen et al. 2012) increased the capabilities of CFD modelling in coastal engineering applications.

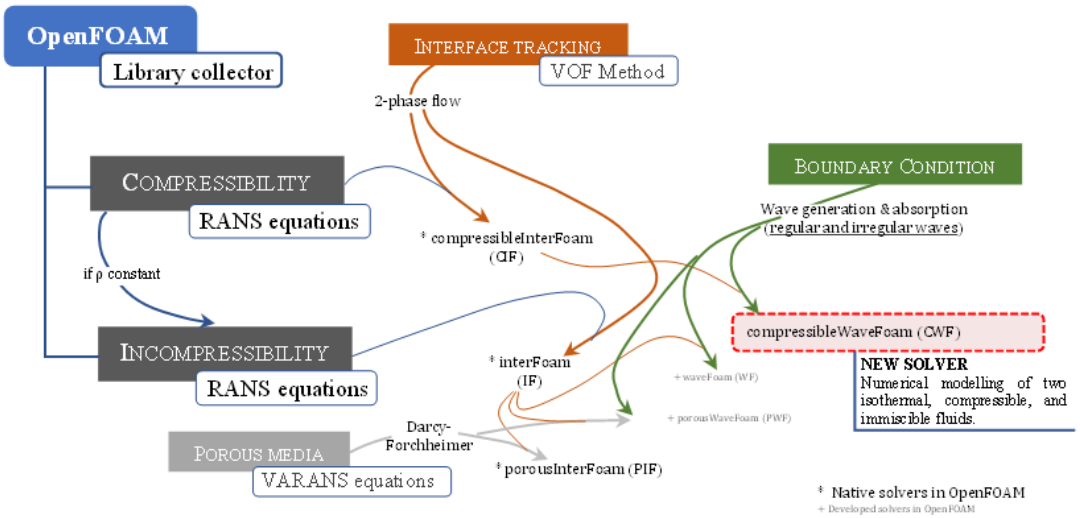

Figure 1. Diagram of elements incorporated in native and user-developed solvers within the OpenFOAM framework. Description of the new solver developed, and numerical modelling capabilities is also shown.

The implementation and the capabilities of CFD modelling in OpenFOAM mainly focuses on incompressible fluid conditions, which include solvers for the simultaneous simulation of 2-phase flows, porous media, and wave generation. The new solver isoCompressibleWaveFoam (CWF) considers: i) the implementation of the mass (Eq. 4) and the momentum (Eq. 5) equations for compressible fluids with ii) the inclusion of the wave generation/absorption boundary condition developed by Jacobsen et al. (2012), and iii) the transport equation from the VOF method for tracking the fluids interface:

$$\frac{\partial \rho}{\partial t} + \nabla \rho U = 0 \tag{4}$$

$$\frac{\partial \rho U}{\partial t} + \nabla (\rho U U) = -\nabla p + \nabla \mu_{eff} \nabla U + F_s \tag{5}$$

$$\frac{\partial \alpha U}{\partial t} + \nabla (\alpha U) + \nabla \left(U_r \alpha (1-\alpha) \right) = 0 \tag{6}$$

The last term on the left-hand side of Eq. (6) aimed at sharpening the interface (Berberovič et al., 2009), with Ur as the relative velocity between fluid phases (i.e. $U_r = U_{phase1} - U_{phase2}$). Also, any fluid property (Φ), such as density or viscosity, is estimated through the weighted average of fluid phase content within the computational cell volume, i.e. $\Phi = \alpha \Phi_{phase1} - (1-\alpha)\, \Phi_{phase2}$.

At a fist stage, the new solver CWF is developed under the assumption of no porous media. However, correlation between the density changes as a function of the pressure and the temperature T are accounted through the gas equation of state (Eq. 7):

$$p = \rho_{phase2} R_{phase2} T, \tag{7}$$

with R_{phase2} is the specific gas constant (for air, R=287 J/(kg·K)). Assuming that the first fluid phase is water, its density is calculated as $\rho_{water} = \rho_{0,water} + \psi(p - p_0)$, where $\rho_{0,water}$ is the initial water density at initial pressure p_0 and the compressibility term is defined as $\psi = 1/(R_{water} T)$, with R_{water}=462 J/(kg·K). Additionally, to simplify the solver development, the fluids were considered isothermal so that the temperature is assumed constant with 300.15 K.

Numerical model setup

The performance of the numerical model developed (CWF) s verified by reproducing a 2-D laboratory test of waves acting over a smooth and impermeable dike structure with a crown wall at the inshore edge of the berm (Figure 2). The selected test is part of a research carried out at the Hydraulic Laboratory of the University of Bologna and based on physical modelling of wave loads and wave overtopping at crown walls under different sea-states for various geometrical configurations (Formentin et al., 2021). The structure configuration and the wave conditions for the selected test were specifically

defined to provide the most severe impacts at the crown wall. Such conditions were obtained by imposing non-breaking waves above the structure slope and by selecting the case of the berm positioned in correspondence of the sea-level. Figure 2 shows the schematic cross-section of the selected test, with reference to the main geometrical parameters: dike slope 1:2 ($\cot\alpha_d$=2), berm elevation to the bottom of the flume h_c=0.35 m, berm width B=0.30 m, height of the crown wall h_w=0.04 m, total structure freeboard R_c=0.04 m.

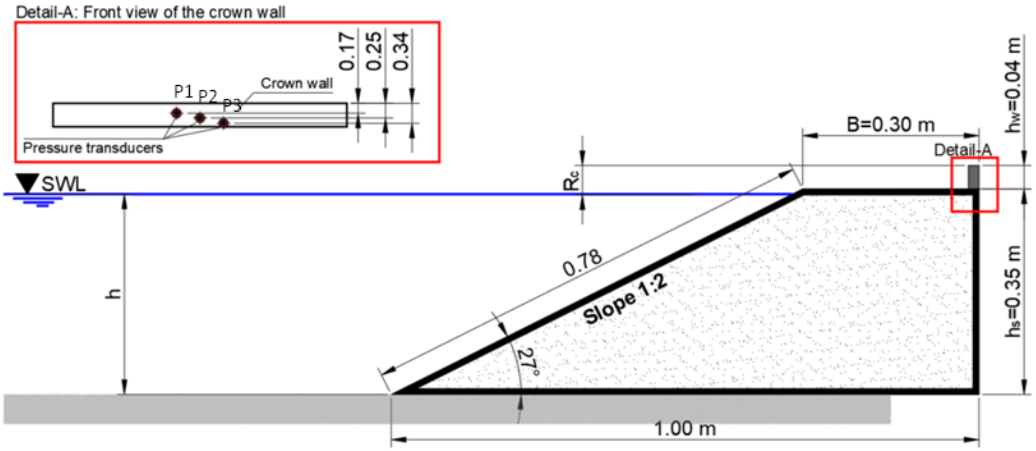

Figure 2. Cross-section of the test selected for the model validation, based on laboratory tests in the Hydraulic Laboratory of the University of Bologna. Features of the dike structure and its crown wall are shown together with the location of pressure transducers (Detail-A). All the measures are in m.

The laboratory test was reproducing with both the new (CWF) and the existing (WF) models to investigate the differences between the compressible and the incompressible solver. Irregular wave conditions based on a Jonswap spectra were implemented within the laboratory test selecting a value of the peak enhancement factor γ=3.3 and imposing target values of the significant wave height H_s=0.05 m and of the peak wave period T_p=1.21 s. Considering the wave conditions targeted and those actually obtained in the laboratory flume, the final wave parameters set up for the model validation were H_s=0.04 m and T_p=1.21-1.22 s, giving a spectral wave steepness $s_{m-1,0}\approx$0.03 and a surf similarity parameter of $\xi_{m-1,0}$>2.88. These conditions were also defined in the numerical simulations.

Irregular waves lead to both high- and low-aerated wave-impacts: the waves that do not break over the slope and propagate over the berm unbroken, directly break against the wall generating high-aerated and violent impacts; vice versa, the waves that break over the slope and/or along the berm have already dissipated most of their energy when hit against the wall and generate low-aerated and modest pressures. Figure 3 provides an example of the two different wave impact conditions obtained with the same laboratory test and generated by two different waves.

Resistant gauges were placed in the wave flume to measure the free-surface level in front of the wave-maker, approximately 1.5 wave lengths away from the wave maker (≈ 5 m) to estimate the wave reflection coefficient K_r. Three pressure transducers were installed in the crown wall to measure the wave pressures at different locations. All the pressure transducers were front-looking and were characterized by a sampling frequency of 1000 Hz and a range of measurement from 70 to 700 mbar. In Figure 2, Detail-A, a front view of the crown wall is given with reference to the horizontal and vertical position of the three pressure transducers P1, P2 and P3.

The positions of the resistant gauges and of the pressure transducers were replicated in the numerical modelling to have correspondence among the numerical and the laboratory data of the free-surface elevation signals and of the wave-induced pressures at the wall. An overtopping tank was positioned behind the structure to estimate the wave overtopping discharge q. The precision in the measurement of the overtopping volumes q was estimated of $1\cdot10^{-5}$ m^3/s (Formentin et al., 2019). The numerical wave overtopping was calculated by time-averaging the instantaneous values of the overtopping volumes behind the crown wall.

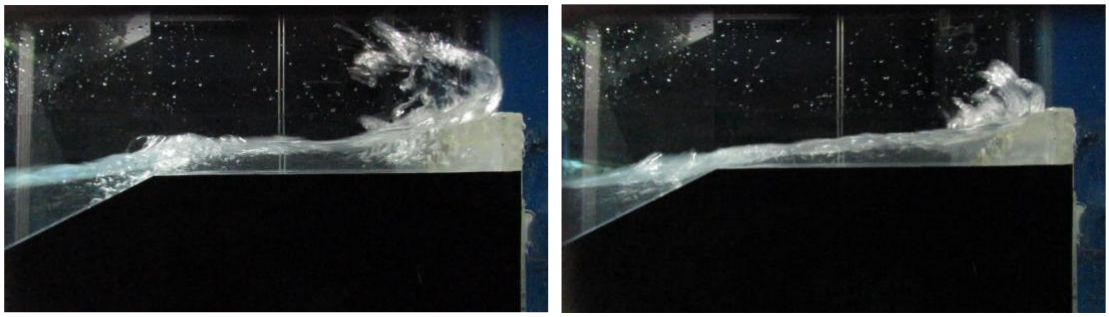

Figure 3. Example of two different wave impact conditions at the crown wall occurring for the same selected test under irregular waves: a) high-aerated condition with a violent wave impact due to direct breaking against the crown wall, and b) low-aerated conditions, where the impact develops after wave braking over the slope and the berm. Pictures taken from the laboratory tests in the Hydraulic Laboratory of the University of Bologna.

For the numerical model verification, the dike structure was assumed as an impermeable body, under slip (CWF) or fixed-value (WF) boundary conditions for velocity, defined based on the numerical model stability. These boundary conditions were also implemented for the *bottom* of the simulated wave flume 12 (length) x 0.5 (wide) x 0.7 (height) m^3, same geometry to that of the laboratory test facility. At the *inlet* and *outlet* boundaries, a relaxation zone scheme was implemented to generate/absorb waves. Open-atmosphere boundary condition was also implemented on the numerical model to simulate flow out of the domain with a zero-gradient condition and an influx based of the velocity in the path-normal direction. Fields of dynamic pressure and velocity were initialized at p_d=0 Pa and U=0 m/s. The dynamic pressure is needed for the assessment of the total pressure as $p=p_d+p_0$, where $p_0=1.03\text{x}10^5$ is obtained following Eq. (7) and an initial air density of 1.2 kg/m^3. For the compressible solver, the temperature field was set to a constant value of 300.15 K for the whole simulation and domain for simplicity of the numerical model testing.

The numerical modelling also considered a bi-dimensional domain for wave propagation over the X-Z plane, so that the lateral boundary conditions of the numerical domain were set to "empty" for both WF and CWF simulations.

RESULTS

Performance and results of the numerical models WF and CWF are hereby assessed in comparison with the laboratory test. Since non-synchronous signals were obtained in the numerical codes with regard to the laboratory test, the performance of the numerical models was assessed by considering statistical or total quantities, such as: the wave height H_s and the wave period T_p obtained in the numerical flume with respect to the target values, the total spectral density, the bulk wave reflection coefficient (K_r), the average wave overtopping discharge (q). Quantitative analysis of the wave-induced pressures developed over the crown wall is also provided to identify the effects of considering compressibility or incompressible conditions in numerical modelling under low- and high-aerated conditions.

A qualitative analysis of the wave impacts, based on image analysis, is finally reported to show and investigate the role of the fluid compressibility on the pressure conditions.

Hydraulic parameters

Comparison of hydraulic parameters among laboratory tests and the numerical models (WF and CWF) is shown in Table 1 based on statistical quantities. The values of H_s, T_p, K_r and of the total reflected wave energy refer to the ones measured/calculated in the physical or numerical channel. All these parameters were calculated by separating the incident and the reflected waves based on the elaboration of the wave signals according to the methodology proposed by Zelt and Skjelbreia (1992).

Table 1. Comparison among LAB-, CWF- and WF-values of characteristic hydraulic parameters associated to the selected tests.

	H_s [m]	T_P [s]	K_r [-]	q [m^3/(sm)]	Total reflected wave energy [$m^2 \cdot s^2$]
LAB	0.047	1.20	0.52	$2.34 \cdot 10^{-4}$	$8.80 \cdot 10^{3}$
WF	0.045	1.26	0.46	$2.81 \cdot 10^{-4}$	$7.92 \cdot 10^{3}$
CWF	0.044	1.22	0.54	$3.37 \cdot 10^{-4}$	$1.10 \cdot 10^{4}$

The wave heights are slightly underestimated by the numerical models, introducing an estimated relative error of 4.3% and 6.3% for WF and CWF, respectively. As for the wave period, an increase of the wave period occurs for the numerical model with variations of 0.8-3.2%, with CWF closer to the target conditions. The WF model underestimated the wave reflection providing an error of 11.5%, whereas the CWF had a slight overestimation of only 3.8% if compared to the laboratory tests. Similarly, the WF and CWF models underestimate and overestimate the total incident wave energy by ~10% and ~15%, respectively. The CWF model was observed to present a redistribution of the reflected wave energy towards lower frequency values with respect to the laboratory tests, which could be possibly related to effects from fluid compressibility. Further testing of the model is needed to properly investigate and assess such phenomenon.

The analysis of the q-values indicates that both the numerical models slightly overestimate the laboratory values, of +20% and +44% for WF and CWF, respectively. This could be explained with the lower value of T_p found in the laboratory tests with respect to the numerical model. However, it should be noted that relative errors up to ± 40% are considered to fall in the standard uncertainty associated to the estimation of the wave overtopping discharge and are in line with the errors associated to the EurOtop (2018) predicting formulae for q and to the most common predicting methods available from the literature, which may often show differences among predictions and measurements greater than the 30%.

Wave-induced pressures

Single wave-induced pressures from laboratory (LAB) and numerical models (WF and CWF) for high- and low- aerated wave impacts are depicted in Figure 4a and 4b, respectively. Main differences are primary observed along the shape of the impact and quasi-static wave components, indicated by the arrows in the charts. For instance, larger oscillations of the pressure signals are developed particularly for the high-aerated load conditions (Figure 4a). These oscillations occurred in a short time interval of 0.1-0.2 s and were mainly noticed for laboratory and CWF tests. In the cases with air compressibility (i.e. LAB and CWF), the oscillations from the impact load are clearly differentiated from the quasi-static load where no peak oscillating pressures are shown. On the contrary, the WF results without air compressibility consideration developed a pulsating load all along the wave passage, i.e., over the impact and the quasi-static load components. This pulsating load is described by a first maximum peak, after which peaks of decreasing magnitude occurred. Additionally, the LAB and the CWF pressure signals described higher peak magnitudes of the impact load, with values ≥0.9 kPa so that, an important underestimation of the peak pressure is noticed for the WF incompressible numerical model, showing a peak of ≈0.7 kPa.

For low-aerated conditions, pulsating loads are developed for all cases (Figure 4b). The peak pressure occurred with a magnitude of ~300-350 Pa for the LAB and CWF tests. The peak pressure is underestimated for the WF numerical model, which described maximum pressures of p≈260 Pa. For the LAB and CWF cases, the first peak pressure is rapidly damped before the development of the quasi-static load. However, by assuming air incompressibility (i.e., WF), oscillations of the pressure signal were developed along the wave passage, similar to the high aerated conditions. This would imply that air pockets interact through the wave impact development and that could not be easily released. Therefore, air compressibility is relevant for the development of the impact load producing oscillations that are rapidly damped by the incoming quasi-static load, which is mostly composed by low aerated water.

By considering incompressibility, the oscillations given by the air phase are not damped, thus representing a condition of larger air entrapment in the water mass during the arrival of the quasi-static load. The latter is not shown in the laboratory tests, leading to the relevance of considering air compressibility for the assessment of wave-induced pressures in high-aerated conditions.

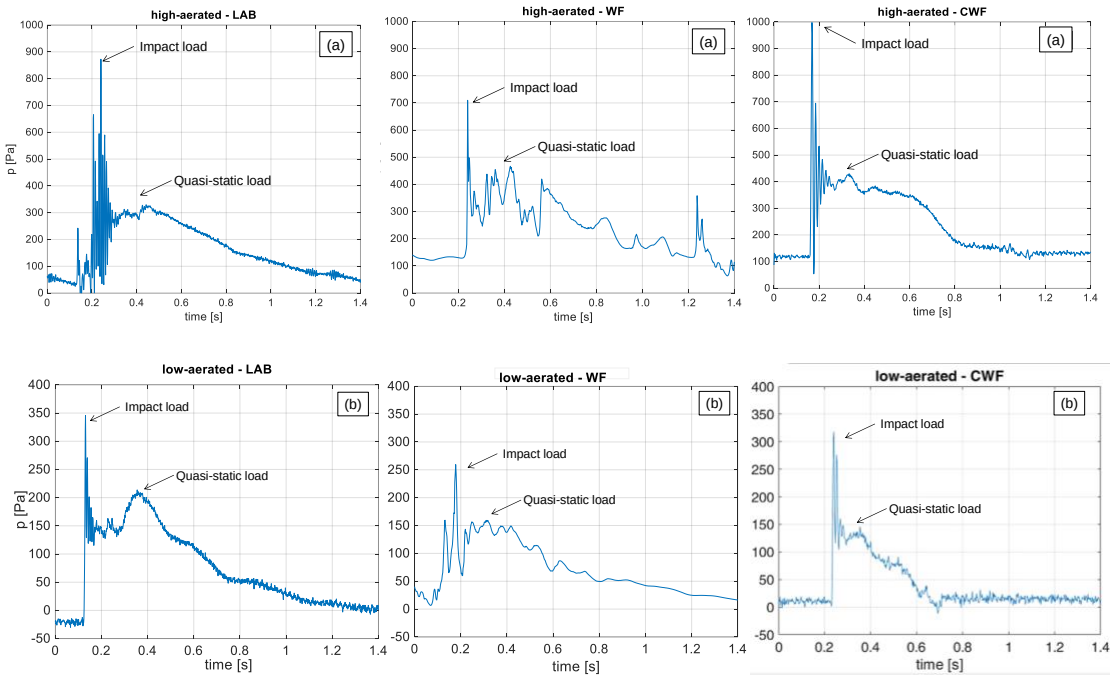

Figure 4. Wave-induced pressures developed at the mid-section of the crown wall for (a) high-aerated and (b) low-aerated wave impacts considering the laboratory conditions ("LAB") and the results from numerical modeling with WF and CWF.

The wave induced pressures changed depending on their location over the crown wall (Figure 5). The higher peak pressure from the impact loads were developed in all cases for the location P2 at the mid-position of the crown wall (see Figure 2-detail A). The impact loads at P2 develops a higher magnitude for the laboratory and CWF cases (Figure 5a, c) than for the WF model (Figure 5b). Additionally, the number of oscillations caused during the impact load are rapidly damped by the incoming quasi-static load. For WF, important oscillations are observed along the passage of the quasi-static load. At the bottom location of the crown wall (P3), the quasi-static wave load produces important wave-induced pressures, but featured by a lower air entrapment, decreasing the oscillations that air compressibility might produce.

The time series of WF shows that the wave pressure signals for P2 and P3 are normally divided by instants of zero pressure between the impact and the quasi-static loads. This reflects the passage of air over the numerical transducer in between, and possibly explained by the effects of air incompressibility that could not be released as shown in the laboratory and CWF model, where the transition is provided by oscillations of pressure (positives and negatives). For the compressibility conditions (i.e., LAB and CWF), instantaneous negative pressures are developed, which could be caused by air detachment from the wall, also increasing the total amplitude of the wave-induced pressure.

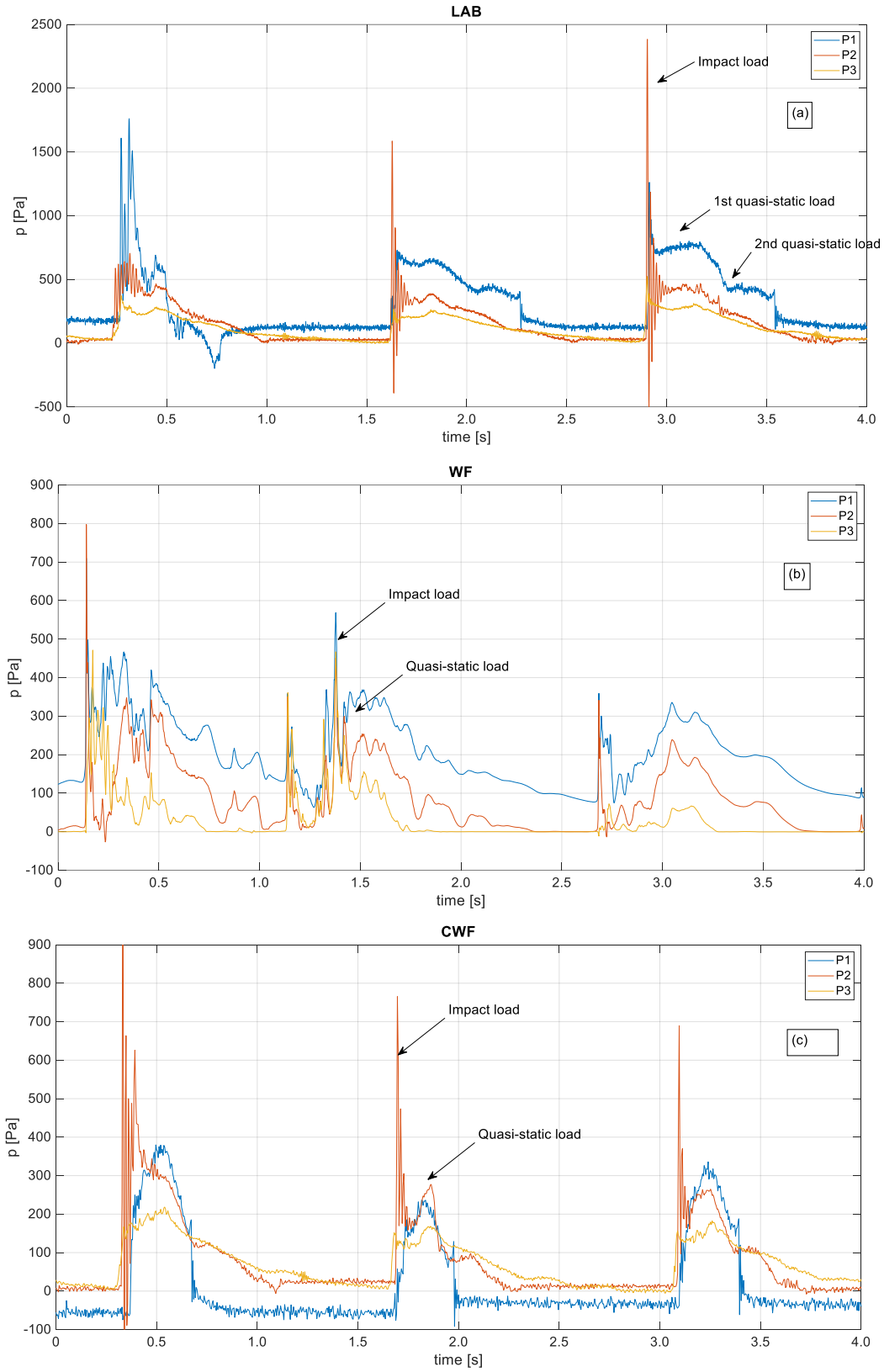

Figure 5. Time series of wave-induced pressures recorded by the pressure transducers at the top (P1), mid (P2) and bottom (P3) position over the crown wall under a high-aerated wave impact condition for (a) laboratory tests, (b) WF and (c) CWF.

For the wave-induced pressures on top of the crown wall (P1), the time series of LAB and CWF describes moments with nearly zero-values, where no air or water produces a change of pressure. A pulsating load dominated by the quasi-static component is noticed in all cases, but with oscillations reduced for the cases where compressibility is considered. For the simulation with air incompressibility, the pressure time series reflects a continuous effect of the air and water at the location of P1. Moreover, oscillations all along the wave pressure signal are noticed in the WF results (Figure 5b). No peak pressures from the impact load are noticed for the CWF model, only leading to the description of a quasi-static load at position P1. A possible underestimation of the pressure magnitude could occur at this location despite the general wave-induced pressure performance in agreement with the experimental data.

The magnitude of the pressures developed during the quasi-static load at P1 is similar between the numerical models (~300-450 Pa) (Figure 5b, c), but underestimating the pressure obtained in the laboratory tests (~500-700 Pa) (Figure 5a). Also, the pressure time series of laboratory tests describes a second quasi-static load for some signals, which were not reproduced by the numerical models and possibly related to the wave overtopping performance considering the location of the pressure transducer P1 on top of the crown wall.

Effects of the aeration on the wave overtopping and impacts

The results of the numerical simulation run with CWF were elaborated also with the software ParaView, which is an open-source platform for qualitative and quantitative data analysis and visualization. Specifically, this software was used to visualize the time-evolution of the wave overtopping and wave impact events, through the graphical rendering of the VOF maps.

An example of the visual analysis offered by the VOF maps is proposed in Figure 6**Figure** , showing a 0.6 s time-evolution of an overtopping event extracted from the numerical simulation of the selected test. The three panels of Figure 6 have been taken in correspondence of the instants $0 \cdot T_p$, $0.25 \cdot T_p$ and $0.5 \cdot T_p$, respectively, and they show the shape of the overtopping tongue and the profile of the free-surface elevation when (a, $0 \cdot T_p$) the wave overturns and impinge on the berm after breaking; (b, $0.25 \cdot T_p$) a second wave front is generated during the turbulent propagation over the berm; (c, $0.5 \cdot T_p$) the wave reaches its maximum run-up height after impacting against the wall.

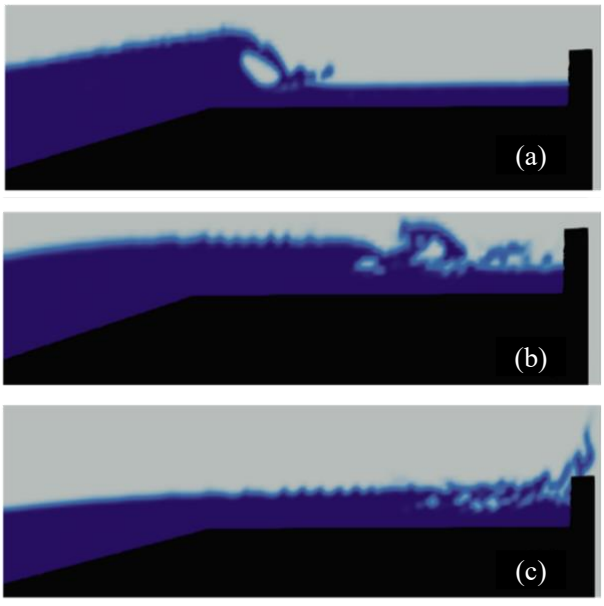

Figure 6. Time-evolution of an overtopping event and detection of the areas of air entrainment for the selected test run with the CWF code.

Figure 6a clearly shows the formation of an air bubble below the wave crest, due to the wave collapsing and consequent breaking above the berm. In this phase, the air phase consists of a single, big, roundly-shaped air pocket. This area evolves into a fragmented amount of smaller bubbles irregularly

shaped, while the wave proceeds over the berm in highly-turbulent conditions. A second, smaller air pocket is generated below the crest of the second wave front (Figure 6b), immediately followed by a bore flow characterized by small bubbles concentrated in the upper part of the water tongue. During the wave impact (Figure 6c), the CWF code shows an irregular shape of the water jet running up the wall and a turbulent flow characterized by small and big air pockets beneath the free-surface in the upper part of the wall. This latter panel suggests that the wave impact occurred in low-aerated conditions considering the lower part of the wall and mid-aerated condition for the upper part. By combining the visual analysis with the quantitative data associated to the VOF time series and to the records of the numerical pressure transducers at P1, P2 and P3, it is possible to correlate the amount of air entrainment with the shape of the pressure traces and the magnitude of the pressure peaks.

Similarly, Figures 6a and 6b suggest that the CWF code could be also applied to investigate quantitatively the amount of the air entrainment during the wave overtopping and the wave breaking, representing therefore a valid support and complement to the experimental analysis.

CONCLUDING REMARKS

The present contribution illustrated and discussed the effects of the air entrapment on the wave pressure loads, investigating the capability and the potentialities of the numerical modelling to catch and reproduce the experimental evidences. To this purpose, a new plug-in solver developed in the OpenFoam environment – isoCompressibleWaveFoam (CWF) – was conceived and developed to model long trains of irregular waves (i.e. at least ≈500 waves) interacting with impermeable and porous structures, solving two compressible, isothermal, immiscible fluids.

Such new solver CWF was applied here to reproduce one laboratory test of wave overtopping and wave impacts against a smooth dike with a crown wall, testing its performance and accuracy in representing the hydraulic and the wave-structure interaction processes, in comparison with the results of the physical tests and of the native solver Waves2Foam (WF) dealing with uncompressible fluids only. CWF resulted to well reproduce the spectrum of the incident waves and to give a fair representation of the wave overtopping discharge, q, with a relative error of ≈40% with respect to the lab value which is comparable to typical uncertainty associated to the numerical models and the literature methods for the prediction of q.

An in-depth analysis of the pressure signals recorded at the crown wall was conducted, to investigate the differences in the representation of pressure trace and values considering (lab and CWF) and disregarding (WF) the air compressibility. Main differences were primary observed along the shape of the impact and quasi-static wave components: for the high-aerated load conditions, the LAB and the CWF showed larger oscillations of the pressure signals occurring in a short time interval and found higher peak magnitudes of the impact load, whereas the WF results developed a pulsating load all along the wave passage and underestimated the pressure peaks. For low-aerated conditions, pulsating loads are developed for all cases, though in the LAB and CWF pressures signals, the first peaks are rapidly damped before the development of the quasi-static load, while the WF described longer, smoothed oscillations of the pressure signal, without significant differences with respect to the case of high-aerated conditions.

Considering the objective impossibility, or hard infeasibility, of getting experimental data on the air entrainment and air density variation, a relevant application of the CWF solver might result in the possibility to punctually quantify the amount of air entrainment during complex phenomena such as the wave breaking and the wave impacts. Indeed, by combining the quantitative values on the air phase and the air density in each cell of the computational domain with the visual analysis of the wave-structure interactions deriving from the graphical rendering of the numerical simulations, it is possible to analyse in details the effects of the air entrainment from the formation of the earliest pockets during the wave breaking to their evolution during the overtopping flow and their role in the wave impacts.

Further testing and broader validation of the new code against smooth and permeable structure is ongoing to release the solver to scientific community.

REFERENCES

Bredmose, H., Bullock, G. and A. Hogg, 2015. Violent breaking wave impacts. Part 3: effects of scale and aeration, *Journal of Fluid Mechanics*, 765, 82–113.

Bullock, G. N., Obhrai, C., Peregrine, D. H. and H. Bredmose, 2007. Violent breaking wave impacts. Part 1: Results from large – scale regular wave tests on vertical and sloping walls, *Coastal Engineering*, 54(8), 602-617.

Cuomo G., Allsop W. and Takahashi S., 2010. Scaling wave impact pressures on vertical walls, *Coastal Engineering*, 57, 604–609.

Engelund F., 1953. On the laminar and turbulent flow of ground water through homogeneous sand. *Trans. Danish academy of Technical sciences*, 3.

Ergun S., 1952. Fluid flow through packed columns. *Chemical Engineering Progress*, 48(2), 89-94.

Formentin S. M., Gaeta M. G., Palma G., Zanuttigh B. and M. Guerrero, 2019. Flow Depths and Velocities across a Smooth Dike Crest, *Water*, 11(10), 2197.

Formentin S.M., Palma G. and B. Zanuttigh, 2021. Integrated assessment of the hydraulic and structural performance of crown walls on top of smooth berms, *Coastal Engineering*, 168, 103951, 18 pp.

Jacobsen, N. G., Fuhrman, D. R. and J. Fredsøe, 2012. A wave generation toolbox for the open-source CFD library: OpenFoam®. *International Journal for numerical methods in fluids*, 70(9), 1073-1088.

Liu S., Gatin I., Obhrai C., Ong M. C. and H. Jasak H, 2019. CFD simulations of violent breaking wave impacts on a vertical wall using a two-phase compressible solver, *Coastal Engineering*, 154, 103564.

Ma Z. H., Causon D. M., Qian L., Mingham C. G., Gu H. B. and P.M. Ferrer, 2014. A compressible multiphase flow model for violent aerated wave impact problems. *Proceedings of the Royal Society A: Mathematical, Physical and Engineering Sciences*, 470(2172), 20140542.

McKenna, J. and W. Allsop, 1999. Statistical distribution of horizontal wave forces on vertical breakwaters, *Coastal Engineering*, 2082-2095.

Peregrine, D. H., Bredmose, H., Bullock, G., Obrhai, C., Müller, G. and G. Wolters, 2005. Water wave impact on walls and the role of air, *Proceedings of 29th International Conference on Coastal Engineering*, ASCE, 4005-4017.

Plumerault, L. R., Astruc, D. and P. Maron, 2012. The influence of air on the impact of a plunging breaking wave on a vertical wall using a multifluid model, *Coastal engineering*, 62, 62-74.

Van Gent, M.R.A. (1995). Porous flow though rubble mound material, *J. of Waterway, Port, Coastal and Ocean Engineering*, 121 (3), 176-181, ASCE, New York.

Zelt J. A. and J. E. Skjelbreia, 1992. Estimating incident and reflected wave field using an arbitrary number of wave gauges. *Proceedings of 23rd International Conference on Coastal Engineering*, ASCE, Venice, vol I, 777–789.